Earthquakes as multiscale dynamic ruptures with heterogeneous fracture surface energy

Satoshi Ide, Hideo Aochi

Earthquakes as multiscale dynamic ruptures with heterogeneous fracture surface energy

Satoshi Ide
Department of Earth and Planetary Science, University of Tokyo, Tokyo, Japan

Hideo Aochi
Service of Land Use Planning and Natural Risks, Bureau de Recherche Géologiques et Minières, Orleans, France

Received 21 December 2004; revised 1 July 2005; accepted 5 August 2005; published 5 November 2005.

[1] We propose a model of the wide-scale growth of dynamic rupture during an earthquake, based on our multiscale simulation of a planar crack in a three-dimensional homogeneous elastic space. A simple slip-weakening law governs the fracture/friction processes, and its characteristic parameters, slip-weakening distance and fracture surface energy, have multiscale heterogeneous distributions. We consider a set of randomly distributed circular patches, whose diameter is proportional to the fracture surface energy. Each patch represents an asperity between irregular fault surfaces, and the size-number relation of the patches obeys power law statistics. We assess rupture propagation from a small instability using a boundary integral equation method with a renormalization technique. Although most events stop shortly after their initiation, some grow, triggering neighboring patches of similar size. Small and large events show statistically self-similar properties of rupture growth and stop spontaneously without requiring a special stopping mechanism. The rupture velocity locally exceeds the shear wave speed but globally remains subshear speed due to the increase of the average fracture energy as the rupture grows. The relation between size and frequency of events is a power law, which is explained by the triggering probability between patches. As a consequence of statistically self-similar random triggering growth, we observe a distinct "main phase" in seismic waves similar to those of natural earthquakes, but we cannot estimate the final size of the event from the initial part of the seismic waves. If this is true for the real earthquakes, predicting the size of a future earthquake would be quite difficult.

Citation: Ide, S., and H. Aochi (2005), Earthquakes as multiscale dynamic ruptures with heterogeneous fracture surface energy, *J. Geophys. Res.*, *110*, B11303, doi:10.1029/2004JB003591.

1. Introduction

[2] Earthquakes are dynamic rupture propagation along fault planes, starting from an elastodynamic instability within a small region. Some earthquakes grow to devastating events while most remain small. This growth process is governed by constitutive laws of fracture/friction of the fault planes, and these laws probably depend on the scale of the phenomena.

[3] Seismic observation suggests that some macroscopic characteristics of earthquakes do not change with size. For example, the ratio between seismically radiated energy E_s and seismic moment M_o is constant or depends only weakly on size [e.g., *Ide and Beroza*, 2001; *Ide et al.*, 2003; *Kanamori and Rivera*, 2004]. E_s and M_o represent dynamic and static sizes of an earthquake, respectively, and quasi-constant E_s/M_o implies the existence of similarity in the earthquake dynamic process. If all earthquakes grow similarly, can an originally small earthquake just randomly grow to a large event?

[4] Several models for wide-scale rupture growth have been proposed. *Fukao and Furumoto* [1985] proposed a random hierarchic rupture growth model, and *Frankel* [1991] calculated the spectrum of seismic waves from a fractal circular patch model. A cascade model is one of the end-members proposed by *Ellsworth and Beroza* [1995] as an interpretation of irregular onsets in observed seismograms. Another end-member is a preslip model where the final earthquake size is explicitly related to the preslip properties. Although there are several numerical studies of dynamic processes following the preslip models [e.g., *Dieterich*, 1992; *Shibazaki and Matsu'ura*, 1992; *Lapusta et al.*, 2000], little has been done concerning numerical calculations of dynamic rupture propagation that are governed by cascade-like slip behavior.

[5] In this paper, we model wide-range rupture growth using a planar crack in a three-dimensional elastic medium with multiscale frictional properties. First, we introduce a circular patch model to represent multiscale frictional prop-

0148-0227/05/2004JB003591$09.00

erties as an analogy of asperities between fault surfaces. Then we carry out numerical simulations of dynamic rupture propagation from a very small instability to spontaneous arrest using a boundary integral equation method (BIEM) with a renormalization technique, introduced by *Aochi and Ide* [2004]. We discuss the statistics and dynamic properties of this model and confirm that this model simulates a physically reasonable triggering sequence of patches whose final size cannot be predicted from the initial stage.

2. Multiscale Friction Model With Circular Patches

[6] Any macroscopic constitutive laws that do not change with scale seem unlikely to simulate wide-range earthquake growth. Both slip-dependent friction laws and rate-and-state friction laws require some distance before reaching dynamic frictional stress. This is called a characteristic distance (or a slip-weakening distance in the slip-weakening model) D_c and the work per unit surface done before the slip reaches D_c is the fracture surface energy G_c. We use a simple slip-weakening friction law as shown in Figure 1. At each point, shear stress increases from the initial value τ_0 to the yielding stress τ_y, then decreases to the residual stress τ_1 linearly as slip increases to D_c. Since the absolute value of τ_1 is independent of the rupture behavior in the case of a planar shear crack, we assume $\tau_1 = 0$. Fracture energy G_c is given as $\tau_y D_c/4$, considering both fault surfaces. We consider the heterogeneous distribution of D_c and G_c as an intrinsic source of scale-dependent frictional property.

[7] The average D_c of large earthquakes is found to be about 0.1–1 m [*Ide and Takeo*, 1997; *Olsen et al.*, 1997; *Mikumo et al.*, 2003]. G_c can be estimated more robustly [*Guatteri and Spudich*, 2000] and is of the order of 1 MJ/m^2 for large earthquakes [*Beroza and Spudich*, 1988; *Ide*, 2003] and is smaller in laboratory experiments by 2–3 orders of magnitude [*Scholz*, 2002; *Ohnaka*, 2003]. G_c increases with crack size in fracture experiments and several mechanisms including microcracking and plastic deformation have been suggested to explain this increasing G_c [e.g., *Lawn*, 1993]. Thus it is probable that average D_c and G_c scale with size at each moment during earthquake rupture growth, although they should be related to some intrinsic material properties.

[8] How can we incorporate increasing G_c in the crack problem? We consider the irregularity of fault plane or fault system as a source of heterogeneous G_c. Topographies of fault planes and fracture surface are generally represented by self-affine fractals [*Brown and Scholz*, 1985; *Okubo and Aki*, 1987; *Scholz*, 2002]. In fact a natural surface is a self-affine fractal for wavelengths shorter than a cutoff length, which *Ohnaka* [2003] related to D_c. Extending this idea, we assign D_c for each asperity on the fault plane depending on its size in the macroscopic fault plane. Here we consider that G_c is proportional to D_c assuming that the stress is homogeneous, namely τ_0 and τ_y are uniform, as demonstrated by *Aochi and Ide* [2004]. This is because the scale dependency of the stress field is not clear for real earthquakes [e.g., *Kanamori and Anderson*, 1975]. At a scale larger than a cutoff length, only the D_c of the cut off length is effective and governs macroscopic frictional behavior, as shown by *Ohnaka* [2003]. Various physical processes including friction, fracture, comminution and abrasion are responsible for the energy consumption during slip, though we call it "fracture energy". We do not discuss which process is dominant in this paper. Rather, as a general idea, we consider that locally consumed fracture energy depends on the linear size of the local asperity, which is also assumed by *Matsu'ura et al.* [1992] in the derivation of their slip-weakening friction law.

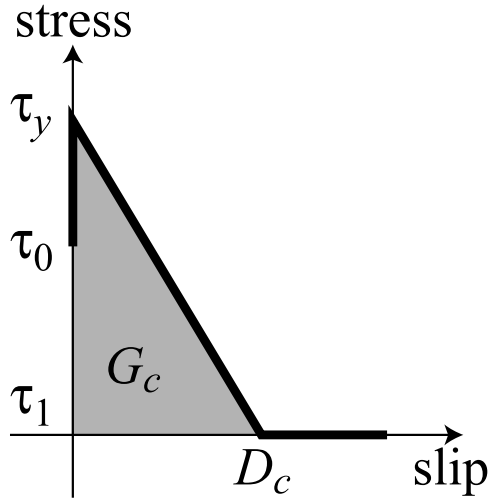

Figure 1. Slip-weakening friction law used in this simulation. Here τ_y, τ_0, τ_1, and D_c are yield stress, initial stress, residual stress and slip-weakening distance, respectively. The shaded area represents fracture energy G_c.

[9] Practically, asperity size is defined at each point on the fault surface topography as the minimum length of a cross section along the macroscopic fault plane (Figure 2a). On the basis of this definition we obtain a corresponding spatial distribution of G_c on a planar fault. Figure 2a is an example of self-affine fractal topography. This topography was made assuming a power spectral decay rate $\beta = 2.5$; β of natural surfaces is generally between 2 and 3 [*Brown and Scholz*, 1985]. G_c is locally defined along this topography as Figure 2b. We further simplify this topography using a set of discrete line segments (Figure 2c). Each segment has G_c that is proportional to the length of the segment and local G_c is defined by the minimum segment that covers the point (Figure 2d). The size and number of line segments obeys a power law whose exponent is related to the fractal dimension of topography.

[10] Since real faults extend in two-dimensional planes, we use circular patches instead of line segments for model calculation. On the basis of the above discussion, we consider a set of circular patches whose radius obeys a power law

$$r_n = 2^n r_0, \tag{1}$$

where r_n is the radius of nth-order patch. The number of patches N_n of this size is expressed as

$$N_n = 2^{-Dn} N_0. \tag{2}$$

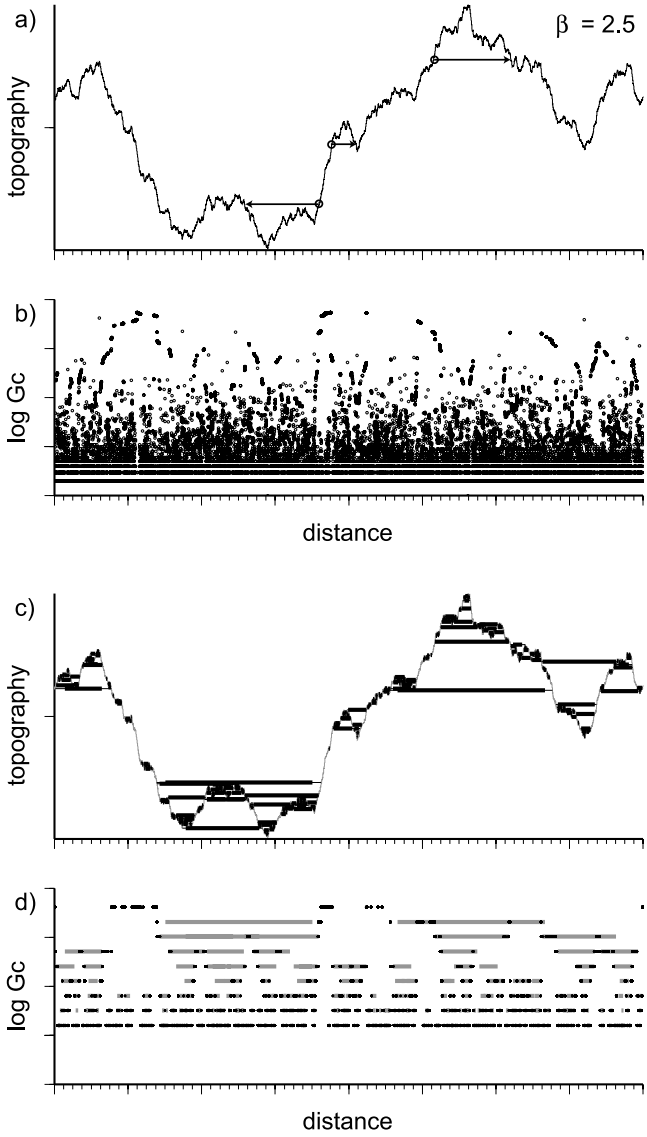

Figure 2. Illustration of relation between topography and G_c distribution assumed in this study. (a) An example of self-affine topography. At each point (circle), the size of asperity is measured as the minimum length of the horizontal section (vector length). (b) Local G_c is proportional to the local size of asperities determined from topography. (c) An approximation of topography using a set of discrete line segments that obey power low statistics. Each segment is drawn at the tip of asperity where the segment can fit. (d) Approximated G_c distribution (black dots) using the segment set (gray lines).

Here D is a constant and it is regarded as a fractal dimension for this size-number relation because the above two equations give the relation

$$N_n \propto r_n^{-D}. \tag{3}$$

Figure 3 is an example of random distribution with 8 orders of circular patches with $D = 2$. In the present paper, we discuss only the case where $D = 2$. In each circular patch, G_c is constant and proportional to the radius. When a point is occupied by multiple patches, G_c of the minimum patch is assigned. It should be noted that the distribution of these patches originates from the irregular topography but we use a planar crack in the following numerical simulations and do not take into account explicit geometrical irregularity.

3. Simulation With the Circular Patch Model

[11] We solve the elastodynamic equation with the spatially heterogeneous friction law and homogeneous stress state. This problem can be treated nondimensionally, but for the purpose of easy comparison to real phenomena, we set the size of the whole model space as 16.384 km × 16.384 km, similar to the width of the seismogenic layer (Figure 3). The minimum (zeroth) and maximum (seventh) radii of the circular patch, r_0 and r_7 are set to 22.5 m, and 2.88 km and their totals are $N_0 = 16384$ and $N_7 = 1$, respectively. D_c of the zero- and seventh-order patches are taken to be 1 mm and 128 mm. Assuming $\tau_0 = 3$MPa and $\tau_y = 5$ MPa loaded in a uniform direction parallel to the horizontal axis of figures, we obtain the G_c of the zero- and seventh-order patches as 1.25 kJ/m^2 and 0.16 MJ/m^2, respectively. The model space is covered by 4096 × 4096 spatial grids (grid size = 4m × 4m), each of which has an intrinsic D_c and a uniform yielding stress τ_y. When a grid point is not covered by any circular patches, we assign a constant D_c for this point. This "background" D_c is 256 mm, which is twice of the D_c of the maximum patch, which means that the whole model space is covered by the eighth-order, infinite patch. Other simulation parameters are taken such that the medium rigidity is 32.4 GPa and the *P wave* and *S* wave velocities are 6.0 and 3.46 km/s, respectively.

[12] Each earthquake rupture starts from an initial small dynamic instability caused by an artificial breakage of one of the zero-order circular patches. We introduce a circular stress-free region with a radius of 15 m in any zero-order patch to make this instability. Since there are numerous zero-order patches (16,384 patches), we are able to discuss the statistical properties by simulating the rupture progress from all the zero-order patches. Before each simulation, the stress field is reset to the homogeneous state. The model space is quite large and it is not realistic to solve the elastodynamic equation in such a space using a normal numerical scheme with a fixed spatial grid size. To solve the problem with limited computational resources, we adopted a boundary integral equation method (BIEM) with a renormalization technique [*Aochi and Ide*, 2004] as explained briefly in the following.

[13] The whole model area is represented by a set of four subspaces as shown in Figure 3. In each subspace, crack propagation is solved using 64 × 64 adjusted spatial grids using the BIEM of *Fukuyama and Madariaga* [1998]. Slip direction is fixed to be the same as the direction of applied stress, namely parallel to the horizontal axis of the figures. All the ruptures first propagate in the smallest subspace (first scale, subspace 256 m × 256 m, grid size 4 m, time step 0.33 ms). Some of them reach one edge of the subspace. Once a rupture reaches the edge, the history of the slip rate is renormalized in a larger spatial grid and a longer time step in the next subspace, whose scale is multiplied by 4, so that the resultant seismic moment release from this earthquake is conserved. We also renormalize D_c

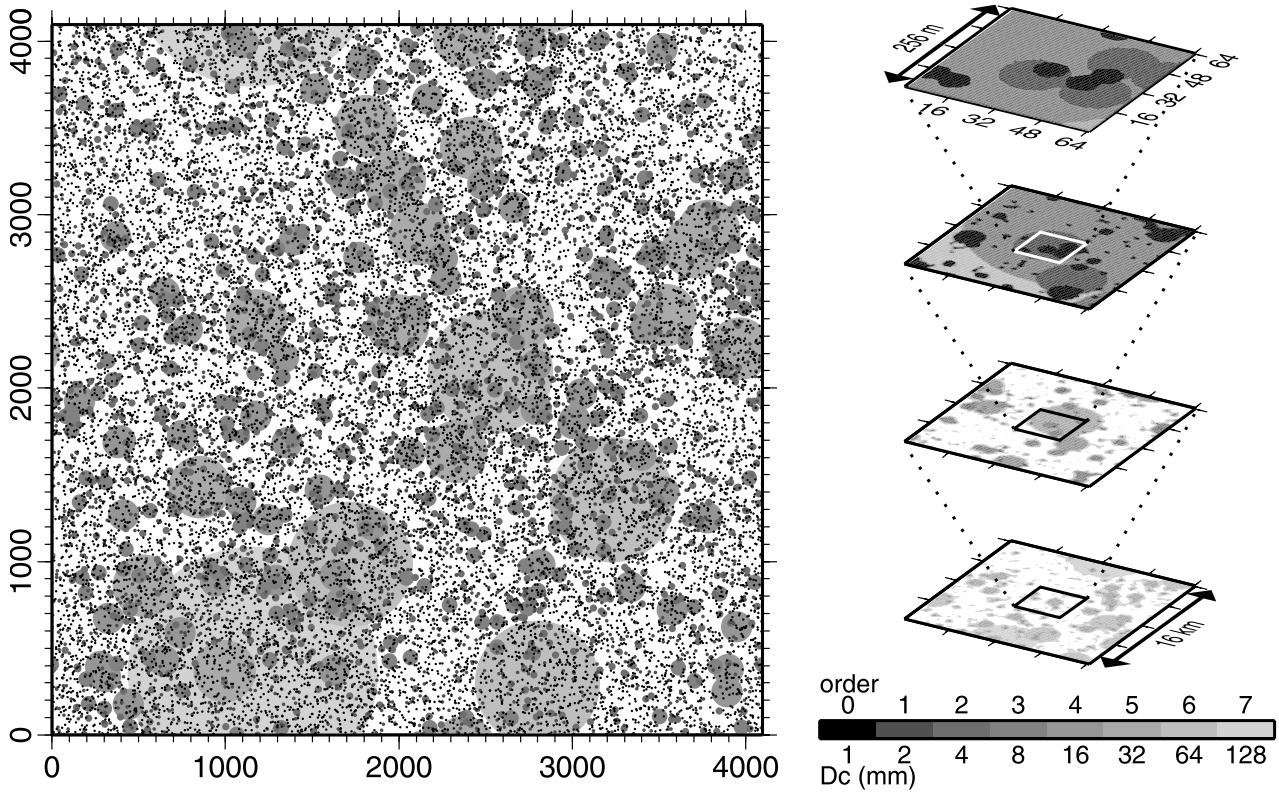

Figure 3. An example of D_c distribution in two dimensions using a set of circular patches. We randomly distribute eight different orders of patches in 4096 × 4096 model space with periodic boundaries, which we consider to be 16 km × 16 km. This model space is treated as four subspaces of different scale through three renormalizations as shown at the right.

and G_c to maintain energy balance. Then the rupture restarts in the second subspace and this procedure is iterated until the rupture stops or reaches the edge of the total model space.

[14] We show the result in the case where there are 16384 zero-order patches in the model space, namely $N_0 = 16384$ and the fractal dimension $D = 2$ (Figure 3). Figure 4 shows the distributions of D_c, final slip distribution, and rupture time in each scale in some examples of simulated dynamic ruptures. In most case, a single rupture process stops shortly after an instability artificially introduced in the zero-order patch without propagating to other patches (Figure 4a). This corresponds to an M_w 1.3 event. The slipped area is restricted within the initial patch. If other patches of zero or first orders are located closely enough to be triggered by dynamic stress accumulation beyond the rupture front, the rupture grows and sometimes enters into the second subspace (Figure 4b). In rare cases, it propagates into the larger scales (Figures 4c and 4d) or does not stop even after breaking the whole space (Figure 4e).

[15] Ruptures breaking the whole space are exceptional, as we will see in the next section. The reason why rupture does not stop is the lack of further hierarchy of larger patches and the moderate value supposed for background D_c. Therefore it should naturally stop if we introduce patches of larger scale or high background D_c.

[16] Since each rupture propagates on a heterogeneous G_c distribution, the rupture process can be quite complex. We observe unilateral, bilateral or circular rupture propagation (directivity) and delayed rupture (subevents), similar to the rupture processes observed in real earthquakes. However, all ruptured patches are connected and there is no distant slip area as is often visible in finite fault models determined by seismic waveform inversion.

4. Frequency-Size Relationship

[17] The relationship between the size (seismic moment) and the cumulative number of events greater than that size roughly follows a power law (Figure 5). In addition to the case $N_0 = 16384$, we simulated two cases with smaller patch numbers, $N_0 = 8192$ and $N_0 = 4096$. All conditions other than the patch number is the same. We note that the fractal dimension of patch distribution is the same ($D = 2$). The rupture of one of the smallest patch alone results in an event of moment magnitude M_w 1.3 and the largest event that breaks whole model space corresponds to about M_w 6. Since we use the discrete sizes of patches, there are inevitably bumps corresponding to each size at M_w 1.3, 1.9, 2.5, 3.1, 3.7, 4.3, 4.9, and 5.5. One may ask a question on the behavior of the largest events, which may seem different from the smaller events in the case of the high density in Figure 5; however, we note that there are not enough events to discuss the statistical significance of any differences. Actually, we find that all these events are related to only one of the 6th patches, which is favorably located within the 7th

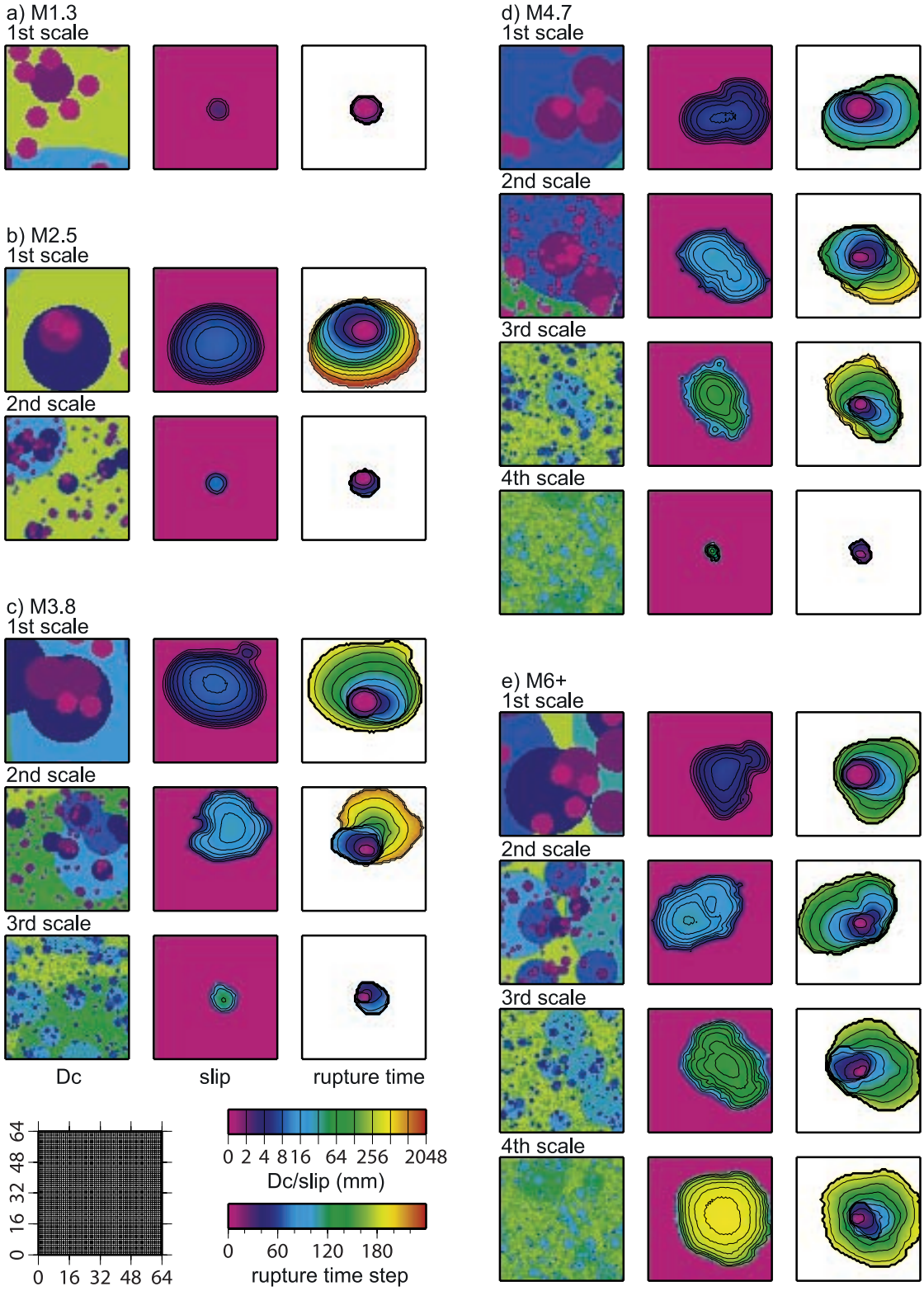

Figure 4. Examples of rupture sequences. In each sequence, the distributions of D_c and slip at the end of calculation (before renormalization), and rupture times in each scale are shown.

patch to make the rupture propagate further on the background. In order to discuss the behavior of the largest event and the effect of our assumption on background D_c, we still need many more simulation examples by investing different heterogeneous patch fields.

[18] The relation for the densest case looks like the Gutenberg-Richter (GR) relation between earthquake magnitude and log frequency with slope (b value) close to 1. However, it should be noted that our result is not simply compared to GR relation because the latter explains seis-

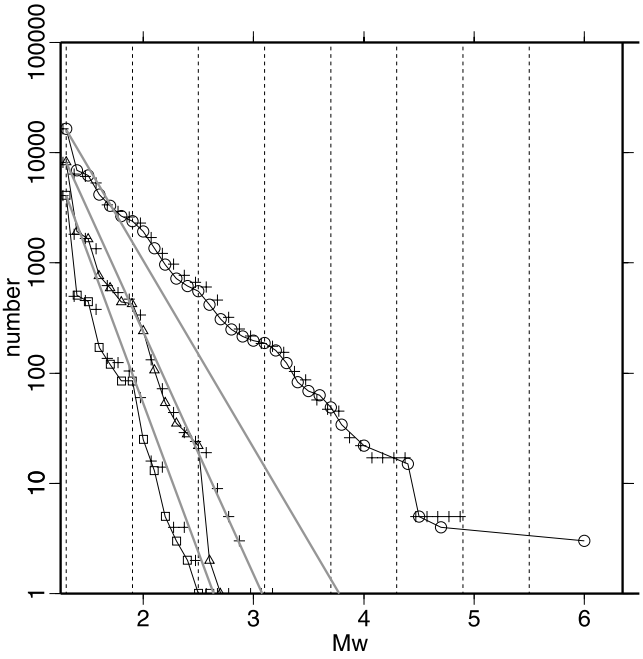

Figure 5. Frequency-magnitude relation. Circles, triangles, and squares connected with lines represent simulation using high-, medium-, and low-density patches, respectively. Crosses are expected value by triggering rules (see text). Gray thick line is a relation suggested by a probabilistic cascading sequence from the smallest patches to larger ones for each calculation. Vertical dotted lines correspond to the magnitude of the assumed patch size.

micity of a particular region during a particular period as a whole system while our calculation does not have any evolution as a system. In our model, each rupture starts from a homogeneous stress condition and a residual stress field after one event is reset before the next calculation so that each simulation is completely independent. Therefore the magnitude-frequency relation provides the probability of event size in the case where the system has evolved to a homogeneous stress state on the fractal fault plane.

[19] This power law can be explained by three simple triggering rules as follows.

[20] 1. A patch triggers another patch of the same or lower orders if they overlap.

[21] 2. An nth-order patch triggers an $(n + 1)$th-order patch when the distance from the peripheral of ruptured area (coalesced patches) to the center of the larger $(n + 1)$th patch is shorter than the radius of the smaller nth patch. In the simple case of two circle patches, this means that the center of the smaller patch is included in the larger patch.

[22] 3. When the total rupture area of coalesced patches of nth order reaches 50% of the area of an $(n + 1)$th-order patch, this coalesced area behaves as an $(n + 1)$th-order patch.

[23] The frequency-magnitude relation calculated numerically based on these rules using the same distribution of circular patches yields quite similar result to that of dynamic simulation (crosses in Figure 5).

[24] Let us consider only the triggering of larger patches by the second rule, which is cascade triggering from the smallest patch to the larger ones. The probability that an $(n - 1)$th-order patch triggers the nth-order patch, f_n, is given as

$$f_n = N_n \pi r_n^2 / S = 2^{(2-D)n} \pi N_0 r_0^2 / S = 2^{(2-D)n} f_0 \tag{4}$$

where f_0 is the ratio of the total area of all zero-order patches to model area S. When $D = 2$ as shown in the above simulations, f_0 is a constant and is 0.024, 0.048, and 0.096 for the low-, medium-, and high-density cases, respectively. The cumulative frequency of events equal to or larger than the size of the nth-order patch, N_n^E, is

$$N_n^E = N_0 \prod_{i=1}^{n} f_i. \tag{5}$$

Taking the common logarithm,

$$\begin{aligned} \log N_n^E &= \log N_0 + \sum_{i=1}^{n} f_i \\ &= \log N_0 + n \log f_0 + \frac{(2 - D) n (n + 1) \log 2}{2}. \end{aligned} \tag{6}$$

From the definition of moment magnitude, $n = (M_n - M_0)/2\log 2$, the expected slope from this triggering mechanism is $\log f_0/2\log 2$ in the case of $D = 2$. For example, the slopes are -2.7, -2.2, and -1.7, for the low-, medium-, and high-density cases in Figure 5, respectively. These values explain the observed trend in the low- and medium-density cases, while the observed slope is more gradual in the high-density case. This means that the interaction between patches of the same size (the third rule) play an important role when the patch density is high.

5. Rupture Propagation

[25] We discuss some aspects of our dynamic rupture propagation in comparison with other well-known rupture behaviors such as rupture propagation with homogeneous G_c and self-similar rupture.

[26] When G_c is homogeneous, no dynamic instability occurs if the crack size is smaller than a critical size determined by G_c and the surrounding stress state. This is also true within the smallest patch in this model. Each rupture starts from an artificially introduced initial instability which is larger than the critical crack size of the zero-order patch. However, this initial rupture is arbitrary and we can take its size as small as laboratory scale if we introduce smaller subspaces. The effect of such a process would be negligible as shown in the simulation of the self-similar rupture model [*Aochi and Ide*, 2004] in which the effects of the initial crack gradually disappear. In our simulation, the size of the artificial initial crack is irrelevant to the consequent rupture behavior such as the rupture propagation velocity and the final rupture area after the initial rupture interacts with neighboring patches. Essentially this model does not require any rupture nucleus related to the characteristics of the source area.

[27] The rupture velocity is determined by the balance between crack extension force G and fracture energy G_c at the crack tip [e.g., *Freund*, 1990]. G increases with crack size and when it is larger than G_c, the rupture velocity increases and eventually reaches a terminal value, which can be the velocity of the Rayleigh wave, S wave or P wave, depending on the stress condition. Figure 6 shows the

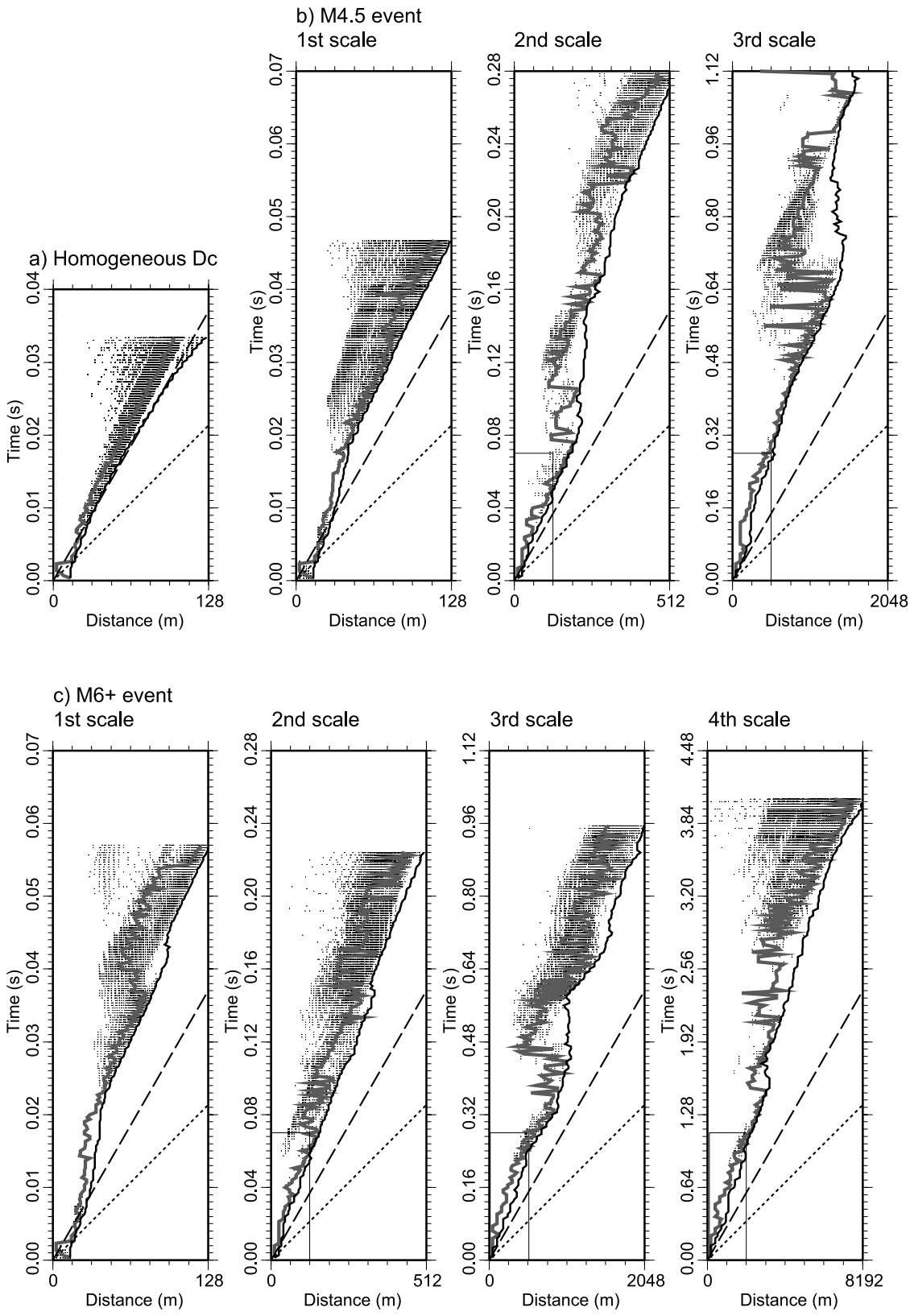

Figure 6. Thick solid lines show the location of rupture front in space (distance from the hypocenter)-time plot. Gray lines represent the location of the maximum velocity. Dotted lines and dashed lines show the *P* and *S* wave velocities, respectively. Dots represents slipping area with slip rates faster than 25% of the maximum in each scale. (a) Homogeneous D_c distribution. (b) and (c) Patch models. Small rectangle box means that the previous scale is renormalized into the box.

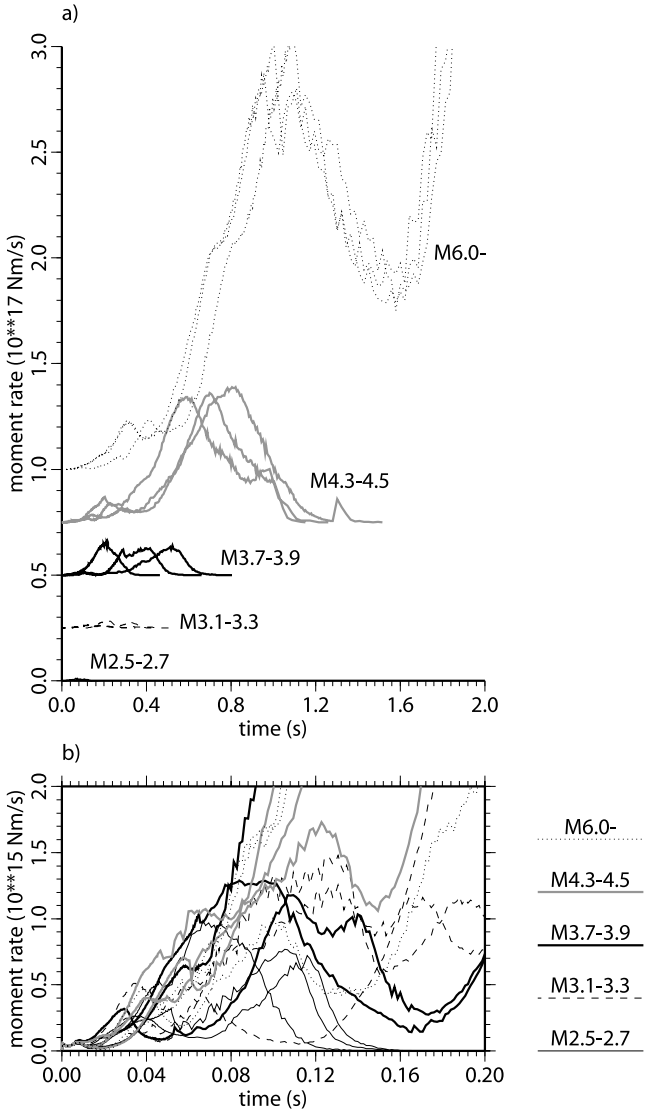

Figure 7. (a) Moment rate functions for events of different sizes. Baselines of different sizes have offsets. (b) Comparison of the first 0.2 s of all functions. Different line types represent different sizes.

temporal evolution of rupture front for homogeneous G_c model (Figure 6a), an M_w 4.5 event (Figure 6b), and a nonstopped event larger than M_w 6 shown by Figure 4e (Figure 6c).

[28] When G_c is homogeneous, rupture first propagates at the Rayleigh wave speed and then it is accelerated to a supershear velocity, up to the P wave velocity under a highly loaded uniform stress field [*Andrews*, 1976; *Madariaga and Olsen*, 2000]. This is reproduced in Figure 6a using the first scale with D_c = 1 mm, that is, of the zero-order patch. Rupture speed exceeds the S wave velocity at about 0.03 s. Although such supershear rupture velocity is common in numerical simulation of dynamic rupture propagation, it is rarely observed for natural earthquakes [*Bouchon et al.*, 2002; *Sekiguchi and Iwata*, 2002; *Rosakis*, 2002].

[29] When we introduce a heterogeneous distribution of G_c, the average rupture velocity is much smaller. We still observe some high-speed rupture locally. For example, there is high-speed rupture similar to Figure 6a in the third scale of Figure 6c at 0.64 s. However, rupture velocity is accelerated or decelerated depending on the surrounding G_c and such high-speed rupture is restricted to a small space and in a short time period. The rupture velocity is approximately constant similar to a self-similar rupture model where G_c is proportional to the distance from the hypocenter. In our model, effective G_c increases almost linearly because patches of larger G_c are broken as rupture propagates and average G_c over the ruptured patch increases. Hence the rupture propagation looks statistically self-similar.

[30] Stopping a spontaneously propagating rupture in a homogeneous stress condition has been a problem in earthquake mechanics. In many studies of dynamic crack propagation, it is a common assumption that the yield stress outside of the model area is very high. Without such a strong boundary, some special mechanisms are necessary, for example, dynamic branching [*Kame and Yamashita*, 1999a, 1999b, 2003] and preexisting fault geometry [*Aochi and Fukuyama*, 2002]. Unlike the previous studies, randomness and multiscale irregularity stop the ruptures in the present model. Every rupture eventually stops because it encounters an unbreakable large G_c area somewhere within the model area. Although the microscopic physical process is not clarified in this study, it is natural that some randomness and multiscale irregularity exists in real fault systems and works as a stopping mechanism.

6. Seismic Waves and Initial Phase

[31] Figure 7 shows the calculated moment rate functions in the fault normal direction from several rupture events of different size. These are proportional to the far-field displacement in a homogeneous infinite elastic medium. Although large events radiate larger seismic waves, the initial part of these waveforms are similar to those of smaller events, and we cannot estimate the final size of each event just from the initial part (Figure 7b). This is because every event in this model is represented by a statistically self-similar random triggering sequence of circular patches and therefore radiated seismic waveforms look self-similar, too. This self-similarity is consistent with the observation of the very beginning of seismic waves of natural earthquakes, which have revealed that both small and large events start with abrupt onsets in seismic records [*Mori and Kanamori*, 1996; *Ellsworth and Beroza*, 1998].

[32] In seismic waves from natural earthquakes we quite often observe a distinct "main phase" corresponding to the main moment release during an event, and the delay of the phase from the onset timescales with the magnitude of the event [*Umeda*, 1990; *Ellsworth and Beroza*, 1995]. We may pick such a phase at the time corresponding to the beginning of the rupture of the largest patch in each dynamic simulation. The leading decrease of wave amplitude makes this phase prominent. Such a decrease is the result of temporary deceleration of the rupture propagation velocity when the rupture front enters the high G_c region of the largest patch. It is obvious that the duration scales with the magnitude because our model is statistically self-similar. Figure 8 shows the relation between magnitude (seismic

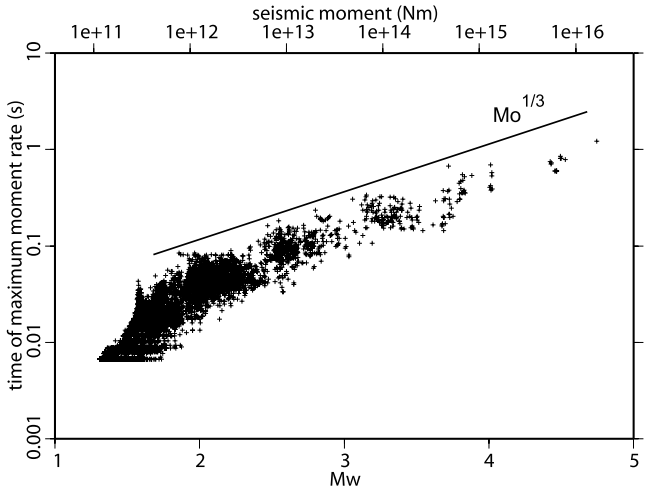

Figure 8. Comparison between magnitude (seismic moment) and time of the maximum moment rate for all events in the simulation. Black line represents proportionality to cubic root of seismic moment.

moment) and the time of the maximum moment rate measured from the beginning for events in the simulation with high-density patches. Except for events smaller than M2 for which the effect of initial artificial rupture remains, this time scales with the cubic root of seismic moment.

[33] If there is a characteristic single value of D_c, we need a rupture nucleus, or preslip, before spontaneous dynamic rupture propagation and the size of preslip area scales with the delay of the main phase. Both the preslip models [*Dieterich*, 1992; *Shibazaki and Matsu'ura*, 1992] and the present model exhibit a similar delay of the main phase. Therefore, although the delay of the main shock is always visible in seismic observations, it is not a suitable measure to distinguish between two models.

7. Conclusion

[34] We successfully simulated wide-scale earthquake growth using simple assumptions: homogeneous stress state and multiscale G_c (D_c) distribution expressed by random circular patches. Each rupture starts from an instability within one of the smallest patches and sometimes propagates triggering other larger patches. Because the average G_c almost linearly increases with the rupture size, the average rupture velocity is smaller than the S wave velocity. Each rupture stops without a special mechanism. Since each rupture is essentially a triggering sequence, seismic waveforms from small and large events cannot be distinguished from the initial part, as is sometimes reported for natural earthquakes.

[35] We assumed that such a G_c distribution follows the fractal property of fault systems and fault topography. The earth crust has fractal properties and every fault trace is terminated by some strong geographic irregularities. However, the quantitative relation between such a realization of G_c and microscopic physics remains unsolved and it will be an important issue in the future.

[36] When an earthquake grows in the area where G_c is almost constant, we may observe some characteristic initial phase-dependent on G_c, which may be useful to predict the final size of the earthquake. On the other hand, if stress state and G_c distribution before an earthquake are similar to those in this study, it is almost impossible to predict the size for any particular forthcoming earthquake. In this model every earthquake is a triggering sequence and we cannot distinguish its final size only from the way it starts. Even with the knowledge about the distribution of large asperities, which may be estimated from geological and geophysical information in nature, the route to the rupture of the large asperities is various and hard to predict. These two end-member models of earthquake growth still need verification by seismic observations and modeling incorporating the stress accumulation process.

[37] **Acknowledgments.** We thank John Douglas, two anonymous reviewers, and an Associate Editor for their helpful comments, which improved our manuscript. This model is a realization of "scope-scale-dependent model" that Masao Nakatani proposed. This work is supported by "Special Project for Earthquake Disaster Mitigation in Urban Areas" of Ministry of Education, Sports, Science and Technology in Japan, and by Project RISQSIS "Risques Sismiques (Seismic Risks)" of BRGM in France.

References

Andrews, D. J. (1976), Rupture propagation with finite stress in antiplane strain, *J. Geophys. Res.*, *81*, 3575–3582.

Aochi, H., and E. Fukuyama (2002), Three-dimensional nonplanar simulation of the 1992 Landers earthquake, *J. Geophys. Res.*, *107*(B2), 2035, doi:10.1029/2000JB000061.

Aochi, H., and S. Ide (2004), Numerical study on multi-scaling earthquake rupture, *Geophys. Res. Lett.*, *31*, L02606, doi:10.1029/2003GL018708.

Beroza, G., and P. Spudich (1988), Linearized inversion for fault rupture behavior: Application to the 1984 Morgan Hill, California, earthquake, *J. Geophys. Res.*, *93*, 6275–6296.

Bouchon, M., M. N. Toksöz, H. Karabulut, M.-P. Bouin, M. Dietrich, M. Aktar, and M. Edie (2002), Space and time evolution of rupture and faulting during the 1999 Izmit (Turkey) earthquake, *Bull. Seismol. Soc. Am.*, *92*, 256–266.

Brown, S. R., and C. H. Scholz (1985), Broad bandwidth study of the topography of natural rock surfaces, *J. Geophys. Res.*, *90*, 12,575–12,582.

Dieterich, J. H. (1992), Earthquake nucleation on faults with rate- and state-dependent strength, *Tectonophysics*, *211*, 115–134.

Ellsworth, W. L., and G. C. Beroza (1995), Seismic evidence for an earthquake nucleation phase, *Science*, *268*, 851–855.

Ellsworth, W. L., and G. C. Beroza (1998), Observation of the seismic nucleation phase in the Ridgecrest, California, earthquake sequence, *Geophys. Res. Lett.*, *25*, 401–404.

Frankel, A. (1991), High-frequency spectral falloff of earthquakes, fractal dimension of complex rupture, b value, and scaling of strength on faults, *J. Geophys. Res.*, *96*, 6291–6302.

Freund, L. B. (1990), *Dynamic Fracture Mechanics*, Cambridge Univ. Press, New York.

Fukao, Y., and M. Furumoto (1985), Hierarchy in earthquake distribution, *Phys. Earth Planet. Inter.r*, *37*, 149–168.

Fukuyama, E., and R. Madariaga (1998), Rupture dynamics of a planar fault in a 3D elastic medium: Rate- and slip-weakening friction, *Bull. Seismol. Soc. Am.*, *88*, 1–17.

Guatteri, M., and P. Spudich (2000), What can strong motion data tell us about slip-weakening fault friction laws?, *Bull. Seismol. Soc. Am.*, *90*, 98–116.

Kame, N., and T. Yamashita (1999a), A new light on arresting mechanism of dynamic earthquake faulting, *Geophys. Res. Lett.*, *26*, 1997–2000.

Kame, N., and T. Yamashita (1999b), Simulation of the spontaneous growth of a dynamic crack without constraints on the crack tip path, *Geophys. J. Int.*, *139*, 345–358.

Kame, N., and T. Yamashita (2003), Dynamic branching, arresting of rupture and the seismic wave radiation in a self-chosen crack path modelling, *Geophys. J. Int.*, *155*, 1042–1050.

Kanamori, H., and D. L. Anderson (1975), Theoretical basis of some empirical relations in seismology, *Bull. Seismol. Soc. Am.*, *65*, 1073–1095.

Kanamori, H., and L. Rivera (2004), Static and dynamic scaling for earthquakes and their implications for rupture speed and stress drop, *Bull. Seismol. Soc. Am.*, *94*, 314–319.

Ide, S. (2003), On fracture surface energy of natural earthquakes from viewpoint of seismic observations, *Bull. Earthquake Res. Inst. Univ. Tokyo*, *78*, 1–120.

Ide, S., and G. C. Beroza (2001), Does apparent stress vary with earthquake size?, *Geophys. Res. Lett.*, *28*, 3349–3352.

Ide, S., and M. Takeo (1997), Determination of constitutive relations of fault slip based on seismic wave analysis, *J. Geophys. Res.*, *102*, 27,379–27,391.

Ide, S., G. C. Beroza, S. G. Prejean, and W. L. Ellsworth (2003), Apparent break in earthquake scaling due to path and site effects on deep borehole recordings, *J. Geophys. Res.*, *108*(B5), 2271, doi:10.1029/2001JB001617.

Lapusta, N., J. R. Rice, Y. Ben-Zion, and G. Zheng (2000), Elastodynamic analysis for slow tectonic loading with spontaneous rupture episodes on faults with rate- and state-dependent friction, *J. Geophys. Res.*, *105*, 23,765–23,790.

Lawn, B. (1993), *Fracture of Brittle Solids*, 2nd ed., Cambridge Univ. Press, New York.

Madariaga, R., and K. Olsen (2000), Criticality of rupture dynamics in 3-D, *Pure Appl. Geophys.*, *157*, 1981–2001.

Matsu'ura, M., H. Kataoka, and B. Shibazaki (1992), Slip-dependent friction law and nucleation processes in earthquake rupture, *Tectonophysics*, *211*, 135–148.

Mikumo, T., K. B. Olsen, E. Fukuyama, and Y. Yagi (2003), Stress-breakdown time and critical weakening slip inferred from the source time functions on earthquake faults, *Bull. Seismol. Soc. Am.*, *93*, 264–282.

Mori, J., and H. Kanamori (1996), Initial rupture of earthquakes in the 1995 Ridgecrest, California sequence, *Geophys. Res. Lett.*, *23*, 2437–2440.

Ohnaka, M. (2003), A constitutive scaling law and a unified comprehension for frictional slip failure, shear fracture of intact rock, and earthquake rupture, *J. Geophys. Res.*, *108*(B2), 2080, doi:10.1029/2000JB000123.

Okubo, P. G., and K. Aki (1987), Fractal geometry in the San Andreas fault system, *J. Geophys. Res.*, *92*, 345–355.

Olsen, K. B., R. Madariaga, and R. J. Archuleta (1997), Three-dimensional dynamic simulation of the 1992 Landers earthquake, *Science*, *278*, 834–838.

Power, W. L., T. E. Tullis, S. R. Brown, G. N. Boitnott, and C. H. Scholz (1987), Roughness of natural fault surfaces, *Geophys. Res. Lett.*, *14*, 29–32.

Rosakis, A. (2002), Intersonic shear cracks and fault ruptures, *Adv. Phys.*, *51*(4), 1189–1257.

Scholz, C. H. (2002), *The Mechanics of Earthquake and Faulting*, 2nd ed., Cambridge Univ. Press, New York.

Sekiguchi, H., and T. Iwata (2002), Rupture process of the 1999 Kocaeli, Turkey, earthquake estimated from strong-motion waveforms, *Bull. Seismol. Soc. Am.*, *92*, 300–311.

Shibazaki, B., and M. Matsu'ura (1992), Spontaneous processes for nucleation, dynamic propagation, and stop of earthquake rupture, *Geophys. Res. Lett.*, *19*, 1189–1192.

Umeda, Y. (1990), High-amplitude seismic waves radiated from the bright spot of an earthquake, *Tectonophysics*, *175*, 81–92.

H. Aochi, Development Planning and Natural Risks Division, BRGM, 3 Avenue Claude Guillemin, BP6009, F-45060 Orleans Cedex 2, France.

S. Ide, Department of Earth and Planetary Science, University of Tokyo, 7-3-1, Hongo, Bunkyo, Tokyo, 113-0033, Japan. (ide@eps.s.u-tokyo.ac.jp)